Electrostatic potentials at Cu(In,Ga)Se_2 grain boundaries - experiment and simulations

Sebastian S. Schmidt,[1,*] Daniel Abou-Ras,[1] Sascha Sadewasser,[1,2] Wanjian Yin,[3] Chunbao Feng,[3] and Yanfa Yan[3]

[1] *Helmholtz-Zentrum Berlin für Materialien und Energie, Hahn-Meitner-Platz 1, 14109 Berlin, Germany*

[2] *International Iberian Nanotechnology Laboratory, Avenida Mestre José Veiga s/n, 4715-330 Braga, Portugal*

[3] *Department of Physics and Astronomy, The University of Toledo, 2801 Bancroft Street, Ohio 43606, USA*

(Dated: September 24, 2012)

Abstract

In the present Letter, we report on a combined ab-initio density functional theory calculation, multislice simulation, and electron holography study, performed on a Σ9 grain boundary (GB) in a $CuGaSe_2$ bicrystal, which exhibits a lower symmetry compared with highly symmetric Σ3 GBs. We find an electrostatic potential well at the Σ9 GB of 0.8 V in depth and 1.3 nm in width, which in comparison with results from Σ3 and random GBs exhibits the trend of increasing potential-well depths with lower symmetry. The presence of this potential well at the Σ9 GB can be explained conclusively by a reduced density of atoms at the GB. Considering experimental limitations in resolution, we demonstrate quantitative agreement of experiment and theory.

PACS numbers: 61.72.Mm, 61.05.jp, 88.40.jn, 31.15.A-

Research and development of polycrystalline Cu(In,Ga)Se_2 (CIGSe) based thin-film solar cells has improved their conversion efficiencies to more than 20 % on glass substrates [1] and 18.7 % on flexible polymer substrates [2] in the past few years. This makes these solar cells the most efficient among all polycrystalline thin-film solar cells [3]. Owing to the complexity of the material, the impact of grain boundaries (GBs) in the polycrystalline CIGSe absorber layer on the electronic properties of the solar cells is not understood sufficiently.

In the case of other polycrystalline thin films applied as absorbers in solar cells, such as Si and GaAs, charges at GBs result in band bending and are known to enhance recombination and reduce the conductivity of these thin films by effectively reducing the charge carrier mobility [4–6]. In the case of CIGSe, the presence of charges has been reported as well [7–10]. However, also valence-band offsets resulting in charge-neutral hole barriers have been suggested based on density-functional theory (DFT) calculations [11, 12], which take the particular defect [13] and surface properties [14, 15] of CIGSe materials into account. Such a barrier preventing charge carrier recombination at GBs was also found experimentally at a $\Sigma 3$ GB in a $CuGaSe_2$ (CGSe) bicrystal [16]. Other DFT calculations propose an atomic relaxation at GBs, leading to a shift of deep-level defects into the valence band [17]. Experimental evidence for a lower density of states in the band gap at the GBs was provided by Mönig et al. [18]. Electrical transport studies combined with local charge measurements on CGSe bicrystal samples have led to the picture of thin (few nm) and high (up to about 500 meV) transport barriers at GBs [19]. However, no physical origin for these transport barriers was given by these authors.

In earlier studies, it has been demonstrated that GBs in CIGSe must be discriminated by their symmetry [20–24], which can be expressed by their Σ value [25]. Regarding ab-initio DFT calculations, so far, the main focus has been on highly symmetric $\Sigma 3$ GBs [11, 17].

In the present Letter, we report on a combined ab-initio DFT calculation, multislice simulation, and electron holography study, performed on a $\Sigma 9$ GB in a CGSe bicrystal (the same already studied by Hafemeister et al. [19]), which exhibits a lower symmetry compared with highly symmetric $\Sigma 3$ GBs treated in various recent reports [11, 12, 16, 19]. We find an electrostatic potential well at the $\Sigma 9$ GB of 0.8 V in depth (in contrast to about 0.2 V at a $\Sigma 3$ GB [22]) and 1.3 nm in width. Abou-Ras et al. [26] report that potential wells at GBs correlate with the presence of stoichiometry variations [27]. Here, we show by DFT calculations and multislice simulations that the presence of a potential well at the $\Sigma 9$ GB can

be explained conclusively by a reduced density of atoms at the GB. Considering experimental limitations in resolution, we demonstrate quantitative agreement of experiment and theory.

To obtain a single Σ9 GB in CGSe as a model system for our investigations, a CGSe bicrystal (thickness $\sim 200\,\mathrm{nm}$) was grown on top of a GaAs bicrystal containing a single Σ9 GB by metal organic vapor phase epitaxy [19]. Owing to the epitaxial growth, the orientation relation of the two crystals in GaAs was transferred to the crystal lattices of the two grains of the CGSe bicrystal, as verified by electron backscatter diffraction [28]. The transmission electron microscopy (TEM) sample of the CGSe Σ9 GB was prepared by use of a Zeiss GEMINI 1540 CrossBeam focused ion beam and a final ion-milling treatment with Ar ions.

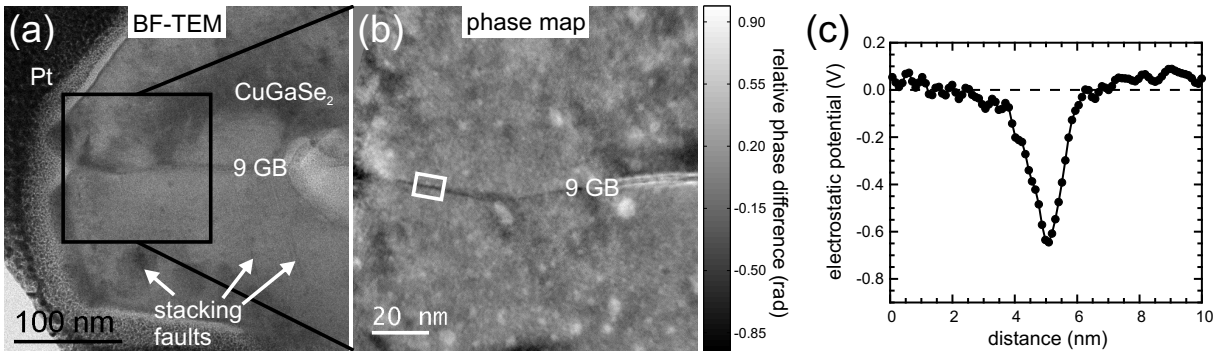

FIG. 1. (a) BF-TEM image of a Σ9 GB in a CGSe bicrystal and (b) corresponding gray-value map of the phase of the object wave function. (c) Measured line profile of differences in the electrostatic potential, extracted from the white box in the phase map. The electrostatic potential in the grain interior was chosen as zero point.

The electrostatic potential at the Σ9 GB in CGSe was investigated by means of inline electron holography in TEM [29]. Local differences in the electrostatic potential within the specimen were determined from local phase differences $\Delta\varphi$ in the (two-dimensional) object wave function of the electron beam after the interaction with the specimen. The reconstruction of the object wave function is based on the acquisition of a through-focal series with a set of 15 images at a LIBRA 200FE transmission electron microscope with an acceleration voltage of $U = 200\,\mathrm{kV}$, followed by the computational procedure described in Ref. [29]. For details, see Ref. [30].

For the acquisition, the plane of the GB was tilted parallel to the optical axis of the microscope. However, it was not possible to acquire high resolution TEM images of both

grains at the same time. Therefore, we concluded that the Σ9 GB plane deviated slightly from the ideal {111} plane, which impeded a perfect edge-on configuration during the measurement. We estimated the deviation from the edge-on configuration from the GB contrast in bright-field TEM (BFTEM) images and the local specimen thickness to be in the range of about $\pm 1 - 2\,^{\circ}$.

The grain boundaries are modeled by an orthorhombic supercell with dimensions of $a = 12.13\,\text{Å}$, $b = 8.06\,\text{Å}$, and $c = 36.77\,\text{Å}$ (see Fig. 2(a) below). It contains 38 Cu, 38 In/Ga and 76 Se atoms. To accomodate the polarity sequence, the supercell contains two oppositely oriented GBs. One of those GBs exhibits a cation-rich (cation core) and the other one an anion-rich (anion core) dislocation core. The boundary planes are formed by rotating the two sides by $90\,^{\circ}$, so the boundary planes are (100) on one side and (001) on the other. The local total potential was calculated using the all-electron WIEN2K [31] code. The muffin-tin radii of Cu, In/Ga, and Se atoms were chosen to be the same, 1.06 Å. We used eight k-points with $(3 \times 5 \times 1)$ division for k point sampling. The parameter of RKMAX [31] is chosen to be 7, which determines the size of the basis set for the matrix. Mesh-grid points of $(100 \times 72 \times 300)$ were used in the orthorhombic cell to calculate the total potential at each point. The potential profile along the c direction was calculated by averaging the potentials over the (a, b) plane.

A BFTEM image of the single Σ9 GB in CGSe and the corresponding relative phase $\Delta\varphi(x, y)$ of the object wave function within the region of interest, highlighted by a black box, are shown in Fig. 1(a) and (b). It is apparent that the phase of the object wave function is lower at the GB compared with the grain interior. The highlighted stacking faults and the fact that the GB does not appear as straight line indicate that there is or was stress acting on the crystal lattices. Further TEM images suggest the presence of a void or a non-contact region of the adjacent grains on the right-hand side of the label "Σ9 GB" in Fig. 1(b). This region has therefore not been evaluated in the present work.

In the framework of the phase object approximation [32], the two-dimensional electrostatic potential $V_{\text{a}}(x, y)$ within the specimen, which is obtained by averaging the three-dimensional electrostatic potential $V(x, y, z)$ along the path of the electrons through the specimen (here: z axis, corresponding to the optical axis), is linked to the phase of the object wave function by [32]

$$\varphi(x,y) = \sigma(U) \int_{\text{path}} V(x,y,z)\,\mathrm{d}z \approx \sigma(U) t(x,y) V_{\text{a}}(x,y), \tag{1}$$

where $t(x,y)$ is the local specimen thickness and $\sigma(U)$ is an acceleration voltage dependent interaction constant ($\sigma(200\,\text{kV}) \approx 7.3 \times 10^6\,\text{V}^{-1}\text{m}^{-1}$). The x and y axes in Eq. 1 are both chosen perpendicular to the z axis. Maps of the local specimen thickness were obtained by [33]

$$t(x,y) = \lambda_{\text{mean}} \ln(I_t(x,y)/I_0(x,y)), \tag{2}$$

where λ_{mean} is the inelastic mean free path of beam electrons within the specimen, $I_t(x,y)$ is the intensity distribution of an unfiltered TEM image, and $I_0(x,y)$ is the intensity distribution of a zero-loss filtered TEM image. The inelastic mean free path of CGSe $\lambda_{\text{mean}}^{\text{CGSe}} \approx 130.4\,\text{nm}$ was estimated by use of an algorithm given in Ref. [33]. With this value, the specimen thickness in the region of interest (white box in Fig. 1(b)) was determined to $47 \pm 2\,\text{nm}$.

From the phase and the thickness map, we extracted approximately 50 individual line profiles perpendicular across the GB (highlighted by the white box in Fig. 1(b)) and averaged them to obtain the corresponding line profile of differences in the electrostatic potential $\Delta V_{\text{a}}(x,y)$ according to Eq. 1, see Fig. 1(c). The error in the electrostatic potential of about 150 mV was estimated from the standard deviation within the flat potential of the grain interior, more than 20 nm away from the GB. Note that the electrostatic potential we measure is caused by all charges within the sample, including atomic nuclei, core electrons, and free charge carriers. The electrostatic potential is about 0.8 V lower at the GB core and the full width at half minimum of this potential well is about 1.3 nm. The presence of electrostatic potential wells at GBs in polycrystalline CIGSe thin films has been found previously for other types of GBs [22, 34]. In good agreement with these earlier reports, the full widths at half minimum in the present work are equally about 1 nm. While highly symmetric $\Sigma 3$ GBs exhibit much smaller depths of the potential wells (about 200 mV [22]), substantially larger values have been found at random GBs ($> 1\,\text{V}$ [22, 26, 34, 35]). Thus, the measured electrostatic potential wells have exhibited so far a trend of increasing depth with lower symmetry.

Surface sensitive Kelvin probe force microscopy (KPFM) measurements [19] at the iden-

tical Σ9 GB as studied in the present work suggested the presence of positively charged donors at the GB and a resulting space charge region, where the correlated potential distribution (depth $\sim 100\,\mathrm{mV}$) extends over a few hundred nm. We note that while KPFM only measures the long-range electrostatic potential owing to a redistribution of free charge carriers, which is caused by charged defects at the GB core, electron holography is in general also sensitive to a local redistribution of nuclei and core or valence electrons on much smaller length scales of a few Å. However, determined by the maximum defocus of about $6\,\mu\mathrm{m}$, only phase relations within approximately 20 nm are meaningful in the present work, and therefore, long-range potentials extending over hundreds of nanometers as measured by KPFM can not be detected. Nevertheless, strong electrostatic potential fluctuations of more than 150 mV around the GB, which may be correlated with band bending, were not detected in the present work.

In order to investigate the occurance and the magnitude of the measured potential well, we performed ab-initio DFT calculations on a crystal model containing two Σ9 GBs in CGSe. Due to the slight deviation of the GB plane from the optimal {111} plane, it was not possible to acquire a high-resolution TEM image showing the crystal lattice of both adjacent grains of the GB at the same time. Therefore, we considered the theoretical structures given in Fig. 2(a) (based on Σ9 GBs determined in SiC), which shows the fully relaxed crystal model with two different GB structures, the cation core and the anion core, as obtained by the ab-initio calculations.

A profile of the differences in the electrostatic potential along the c dimension, averaged in the planes parallel to the GB, was determined from the ab-initio DFT calculations, see Fig. 2(b). This profile clearly exhibits potential wells at the position of both GB cores. A similar potential distribution was obtained across corresponding anion and cation GB cores in $CuInSe_2$ (see Ref. [30]).

The two-dimensional valence-charge density distribution extracted from the DFT calculations (see Ref. [30]) exhibits no substantial differences in the valence and core electron distribution of atoms at the GB and in the grain interior. Therefore, it can be expected that the potential wells at the GB cores are mainly due to the reduced atomic densities visible in Fig. 2(a).

To gain a better insight into the scattering of the electron beam at the CGSe bicrystal and thus the interpretation of the potential well found by electron holography, we performed

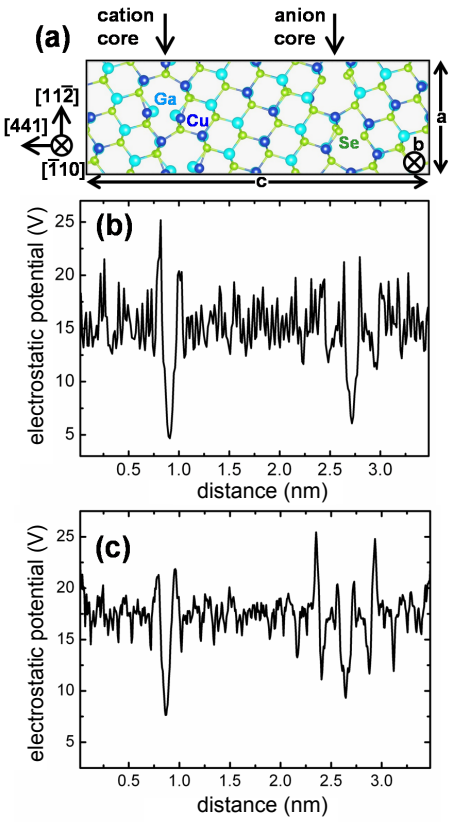

FIG. 2. (a) Crystal model of the CGSe Σ9 GB cores after ab-initio DFT calculations. (b) Calculated electrostatic potential profile by ab-initio DFT calculations across the GB cores. (c) Potential profile from multislice simulations on the fully relaxed crystal model in (a).

multislice simulations on the fully relaxed crystal model by use of the simulation software JEMS [36]. The [110] direction of the CGSe crystal was oriented in parallel to the electron beam and the specifications of our microscope (accelaration voltage, aberrations of the lens, energy spread) were used for the multislice simulations. Scattering factors of neutral atoms (since that for Se^{2-} is not given in the literature) according to Refs. [37, 38] were employed. We determined the averaged electrostatic potential across the GBs (Fig. 2(c)) from the simulated object phase wave function of the electron beam by application of Eq. 1.

Although the potential profiles in Figs. 2(b) and (c) differ slightly in the grain interiors, the widths and depths of the potential wells at the cation and anion GB cores agree well. The difference can be explained by the fact that the DFT calculation accounts for the exact electron density, while the multislice simulation takes into account only the position and the scattering factors of the constituent atoms, which are considered neutral. The depths

$(8 - 10\,\mathrm{V})$ of the potential wells at the GB cores are much larger, while the widths (about 0.2 nm) are much narrower compared with the measurement. One reason for this discrepancy may be the limited spatial resolution of the TEM measurement.

In order to make the potential profile from the multislice simulation comparable to the measured one, we applied a fast Fourier transform low pass filter on the two-dimensional potential image with the spatial cut off frequency of the same value as the size of the objective aperture during the image acquisition. Also, the average value of the simulated potential profile was set to 0 V. The resulting potential profile is shown in Fig. 3(a). Although the lattice structures are equivalent in the case of the anion and the cation core, the atomic species involved in the binding across the GBs are different. Hence, bonding lengths and charge densities are expected to be different in both cases, and likewise the potential well depths. Since the scattering factor of Se is larger than that of Cu and Ga [37, 38], one would expect a smaller potential well depth at a core with a higher density of Se atoms, i.e., the anion core, as found in the present study.

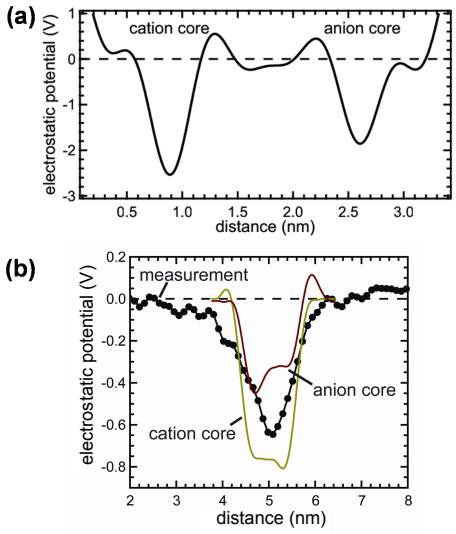

FIG. 3. (a) Multislice-simulated, electrostatic potential profile from Fig. 2(c) after application of a fast Fourier transform low pass filter, corresponding to the objective aperture size during TEM image acquisition. (b) Multislice-simulated, electrostatic potential profiles across the anion and cation GB cores after a tilt of 1.5 °, and the measured potential profile from Fig. 1(c).

Finally, we also take the tilted GB plane into account, assuming a tilt of the supercell with respect to the electron beam of 1.5 °. For this estimation, we approximated the analyzed

region of the specimen by a stack of 58 supercells, to account for its thickness of about 47 nm as measured by TEM (see above). Each supercell is displaced with respect to the others according to the applied tilt angle. Fig. 3(b) shows that our experimental data coincide well with the simulated values of the anion and cation GB cores. Therefore, our results indicate that the potential well we measured at the Σ9 GB in CGSe forms primarily due to a reduced local atomic density, which is found at the fully relaxed GB cores. This reduced atomic density may be correlated with the presence of a neutral barrier of about the same width that was proposed by Hafemeister et al. [19] for the very same GB.

Note that compositional changes at GBs as found by Abou-Ras et al. [26] may also contribute to the measured potential well. However, the absence of any compositional change in our present calculation and simulation showed that the depth and the width of the potential well can be solely explained by the lower atomic density at the GB. In turn, a lower local atomic density may also give a substantial contribution to potential wells measured at other GBs [22, 34].

In conclusion, we showed by application of electron holography in TEM that the electrostatic potential at a Σ9 GB in a model-type CGSe thin film exhibits a well of about 0.8 V in depth in a confined region of about 1.3 nm around the GB core. This result fits well in the trend of deeper electrostatic potential wells for lower GB symmetries. By DFT calculations and multislice simulations, we were able to reproduce the experimental results. Our work showed that one major contribution to the potential well is the reduced density of atoms at the cation and anion GB cores.

The authors would like to thank H. Kropf for the FIB preparation of the TEM lamella and J. Albert, M. Hafemeister, and S. Siebentritt for the growth of the bicrystal. Continuous support by C.T. Koch, University of Ulm, Germany, is gratefully acknowledged.

* sebastian.schmidt@helmholtz-berlin.de

[1] P. Jackson, D. Hariskos, E. Lotter, S. Paetel, R. Wuerz, R. Menner, W. Wischmann, and M. Powalla, Prog. Photovolt: Res. Appl., **19**, 894 (2011), ISSN 1099-159X.

[2] A. Chirilă, S. Buecheler, F. Pianezzi, P. Bloesch, C. Gretener, A. R. Uhl, C. Fella, L. Kranz, J. Perrenoud, S. Seyrling, R. Verma, S. Nishiwaki, Y. E. Romanyuk, G. Bilger, and A. N.

Tiwari, Nat. Mater., **10**, 857 (2011), ISSN 1476-1122.

[3] M. A. Green, K. Emery, Y. Hishikawa, W. Warta, and E. D. Dunlop, Prog. Photovolt: Res. Appl., **20**, 12 (2012), ISSN 1099-159X.

[4] T. I. Kamins, J. Appl. Phys., **42**, 4357 (1971).

[5] J. Y. W. Seto, J. Appl. Phys., **46**, 5247 (1975).

[6] W. Siegel, G. Kühnel, and H. A. Schneider, phys. stat. sol. (a), **87**, 673 (1985), ISSN 1521-396X.

[7] R. Chakrabarti, B. Maiti, S. Chaudhuri, and A. Pal, Sol. Energy Mater. Sol. Cells, **43**, 237 (1996), ISSN 0927-0248.

[8] A. Virtuani, E. Lotter, M. Powalla, U. Rau, J. H. Werner, and M. Acciarri, J. Appl. Phys., **99**, 014906 (2006).

[9] S. Sadewasser, T. Glatzel, S. Schuler, S. Nishiwaki, R. Kaigawa, and M. C. Lux-Steiner, *Proceedings of Symposium B, Thin Film Chalcogenide Photovoltaic Materials, E-MRS Spring Meeting*, Thin Solid Films, **431-432**, 257 (2003), ISSN 0040-6090.

[10] S. Siebentritt and S. Schuler, *13th International Conference on Ternary and Multinary Compounds*, J. Phys. Chem. Solids, **64**, 1621 (2003), ISSN 0022-3697.

[11] C. Persson and A. Zunger, Phys. Rev. Lett., **91**, 266401 (2003).

[12] C. Persson and A. Zunger, Appl. Phys. Lett., **87**, 211904 (2005).

[13] S. B. Zhang, S.-H. Wei, A. Zunger, and H. Katayama-Yoshida, Phys. Rev. B, **57**, 9642 (1998).

[14] J. E. Jaffe and A. Zunger, Phys. Rev. B, **64**, 241304 (2001).

[15] S. B. Zhang and S.-H. Wei, Phys. Rev. B, **65**, 081402 (2002).

[16] S. Siebentritt, S. Sadewasser, M. Wimmer, C. Leendertz, T. Eisenbarth, and M. C. Lux-Steiner, Phys. Rev. Lett., **97**, 146601 (2006).

[17] Y. Yan, C.-S. Jiang, R. Noufi, S.-H. Wei, H. R. Moutinho, and M. M. Al-Jassim, Phys. Rev. Lett., **99**, 235504 (2007).

[18] H. Mönig, Y. Smith, R. Caballero, C. A. Kaufmann, I. Lauermann, M. C. Lux-Steiner, and S. Sadewasser, Phys. Rev. Lett., **105**, 116802 (2010).

[19] M. Hafemeister, S. Siebentritt, J. Albert, M. C. Lux-Steiner, and S. Sadewasser, Phys. Rev. Lett., **104**, 196602 (2010).

[20] D. Fuertes Marrón, S. Sadewasser, A. Meeder, T. Glatzel, and M. C. Lux-Steiner, Phys. Rev. B, **71**, 033306 (2005).

[21] D. Abou-Ras, S. Schorr, and H. W. Schock, Journal of Applied Crystallography, **40**, 841 (2007).

[22] D. Abou-Ras, C. T. Koch, V. Küstner, P. A. van Aken, U. Jahn, M. A. Contreras, R. Caballero, C. A. Kaufmann, R. Scheer, T. Unold, and H.-W. Schock, Thin Solid Films, **517**, 2545 (2009), ISSN 0040-6090.

[23] M. Kawamura, T. Yamada, N. Suyama, A. Yamada, and M. Konagai, Jpn. J. Appl. Phys., **49**, 062301 (2010).

[24] R. Baier, D. Abou-Ras, T. Rissom, M. C. Lux-Steiner, and S. Sadewasser, Appl. Phys. Lett., **99**, 172102 (2011).

[25] H. Grimmer, W. Bollmann, and D. H. Warrington, Acta Cryst. A, **30**, 197 (1974).

[26] D. Abou-Ras, S. S. Schmidt, R. Caballero, T. Unold, H.-W. Schock, C. T. Koch, B. Schaffer, M. Schaffer, P.-P. Choi, and O. Cojocaru-Mirédin, Adv. Energy Mater., **2**, 992 (2012), ISSN 1614-6840.

[27] D. Abou-Ras, B. Schaffer, M. Schaffer, S. S. Schmidt, R. Caballero, and T. Unold, Phys. Rev. Lett., **108**, 075502 (2012).

[28] M. Hafemeister, S. Siebentritt, S. Sadewasser, C. Frank-Rotsch, and M. C. Lux-Steiner, in *Mater. Res. Soc. Symp. Proc.*, Vol. 1012 (Materials Research Society, 2007) pp. 327–332.

[29] C. T. Koch, Ultramicroscopy, **108**, 141 (2008), ISSN 0304-3991.

[30] "See the supplemental material at http://link.aps.org/-supplemental/10.1103/physrevlett.109.095506 for experimental details of the inline electron holography analysis in tem and additional data from dft calculations.".

[31] P. Blaha, K. Schwarz, G. K. H. Madsen, D. Kvasnicka, and L. J., "WIEN2K: An Augmented Plane Wave and Local Orbital Program for Calculating Crystal Properties," (2001).

[32] L. Reimer, *Transmission Electron Microscopy*, 4th ed. (Springer-Verlag, 1997).

[33] R. F. Egerton, *Electron Energy-Loss Spectroscopy in the Electron Microscope* (Plenum Press, New York, 1996).

[34] D. Abou-Ras, J. Dietrich, J. Kavalakkatt, M. Nichterwitz, S. Schmidt, C. Koch, R. Caballero, J. Klaer, and T. Rissom, *Special Issue : Thin film and nanostructured solar cells*, Sol. Energy Mater. Sol. Cells, **95**, 1452 (2011), ISSN 0927-0248.

[35] S. S. Schmidt, *Microscopic properties of grain boundaries in Cu(In,Ga)Se_2 and $CuInS_2$ thin-film solar cells studied by transmission electron microscopy*, Ph.D. thesis, Technical University,

Berlin (2011).

[36] P. A. Stadelmann, Ultramicroscopy, **21**, 131 (1987), ISSN 0304-3991.

[37] D. Rez, P. Rez, and I. Grant, Acta Crystallogr. Sect. A, **50**, 481 (1994).

[38] L.-M. Peng, Acta Crystallogr. Sect. A, **54**, 481 (1998).